

promoting access to White Rose research papers



Universities of Leeds, Sheffield and York
<http://eprints.whiterose.ac.uk/>

This is an author produced version of a paper published in **Quaternary Science Reviews**.

White Rose Research Online URL for this paper:

<http://eprints.whiterose.ac.uk/77904/>

Paper:

Glasser, NF, Davies, BJ, Carrivick, JL, Rodés, A, Hambrey, MJ, Smellie, JL and Domack, E (2014) *Ice-stream initiation, duration and thinning on James Ross Island, northern Antarctic Peninsula*. *Quaternary Science Reviews*, 86. 78 - 88.

<http://dx.doi.org/10.1016/j.quascirev.2013.11.012>

1 **Ice-stream initiation, duration and thinning on James Ross Island, northern**
2 **Antarctic Peninsula**

3

4 N.F. Glasser^{1†}, B.J. Davies¹, J.L. Carrivick², A. Rodes³, M.J. Hambrey¹, J.L. Smellie⁴,
5 E. Domack⁵

6 ¹Department of Geography and Earth Sciences, Aberystwyth University, Wales,
7 SY23 3DB, UK.

8 ²School of Geography, University of Leeds, LS2 9JT, UK

9 ³SUERC, East Kilbride, UK

10 ⁴Department of Geology, University of Leicester, University Road, Leicester LE1
11 7RH, UK

12 ⁵Department of Geosciences, Hamilton College, Clinton, New York 13323, USA

13 †Email: nfg@aber.ac.uk

14

15 **ABSTRACT**

16 Predicting the future response of the Antarctic Ice Sheet to climate change requires
17 an understanding of the ice streams that dominate its dynamics. Here we use
18 cosmogenic isotope exposure-age dating (²⁶Al, ¹⁰Be and ³⁶Cl) of erratic boulders on
19 ice-free land on James Ross Island, north-eastern Antarctic Peninsula, to define the
20 evolution of Last Glacial Maximum (LGM) ice in the adjacent Prince Gustav Channel.
21 These data include ice-sheet extent, thickness and dynamical behaviour. Prior to ~18
22 ka, the LGM Antarctic Peninsula Ice Sheet extended to the continental shelf-edge
23 and transported erratic boulders onto high-elevation mesas on James Ross Island.
24 After ~18 ka there was a period of rapid ice-sheet surface-lowering, coincident with
25 the initiation of the Prince Gustav Ice Stream. This timing coincided with rapid

26 increases in atmospheric temperature and eustatic sea-level rise around the
27 Antarctic Peninsula. Collectively, these data provide evidence for a transition from a
28 thick, cold-based LGM Antarctic Peninsula Ice Sheet to a thinner, partially warm-
29 based ice sheet during deglaciation.

30

31 **INTRODUCTION**

32 The Antarctic Peninsula is one of the most rapidly warming areas of the Earth
33 (Turner et al., 2005, Vaughan et al. 2003), with warming and snow-melt rapidly
34 accelerating over the last century (Abram et al., 2013), increases in precipitation
35 (Turner et al., 2009), a longer melt season (Barrand et al., 2013) and enhanced
36 moss growth and microbial activity (Royles et al., 2013). The north-eastern Antarctic
37 Peninsula is sensitive to even small changes in atmospheric temperature, with
38 glacier acceleration, thinning and recession, and the collapse of several large ice
39 shelves observed in recent decades (Cook et al. 2005, 2010; Pritchard et al., 2012).

40

41 Documented changes in Antarctica also include the rapid and dynamic fluctuations of
42 the Siple Coast ice streams (Joughin et al. 2002) and the recent recession,
43 acceleration and thinning of Pine Island Glacier (Pritchard et al., 2012). Increased
44 discharge of cold water from shrinking ice shelves has also been related to increases
45 in the extent of Antarctic sea ice, which may offset projected future precipitation
46 increases around Antarctica in a warming climate (Winkelmann et al., 2012; Bintanja
47 et al., 2013). Oceanic warming in Antarctica has been linked to increases in the
48 upwelling of warm Circumpolar Deep Water, which melts tidewater glaciers and ice
49 shelves from below (Pritchard et al., 2012). Upwelling of Circumpolar Deep Water, in
50 association with El Niño–Southern Oscillation (ENSO) and Southern Annular Mode

51 climatic oscillations, is projected to continue, raising questions regarding the dynamic
52 response of ice sheets and ice streams to these changes.

53

54 Predicting the wider future response of the Antarctic Ice Sheet to climate change
55 therefore requires understanding of the ice streams that dominate its dynamics.
56 Changes in dynamical ice-stream behaviour are a first-order control on rates of
57 deglaciation and meltwater discharge to the oceans, both now and in the immediate
58 future (Gregoire et al., 2012). Although there is abundant marine geological evidence
59 that, at the Last Glacial Maximum (LGM), the Antarctic Peninsula Ice Sheet was
60 drained by ice streams (Davies et al., 2012a), little is known about ice-stream
61 dynamical behaviour, including the timing of ice-stream initiation, ice-stream duration
62 and the rate of ice-stream thinning (Livingstone et al., 2012). Marine geological
63 studies (for example, Ó Cofaigh et al. 2005, 2008; Graham and Smith 2012) also
64 provide only a snapshot of ice-stream behaviour during deglaciation (Bentley and
65 Anderson, 1998; Evans et al., 2005, Heroy and Anderson, 2007; Graham et al.
66 2009).

67

68 Constructing ice sheet chronologies from marine geological evidence is problematic
69 because of the large marine reservoir effect that hinders radiocarbon dating (Davies
70 et al., 2012a). An alternative approach in Antarctica is to use isolated coastal and
71 inland nunataks as “dipsticks” to measure vertical changes in the ice sheet using
72 cosmogenic nuclide methods (Bentley et al., 2006; Mackintosh et al., 2007; Balco et
73 al., 2011, 2013). This dipstick approach has yielded important data about vertical
74 changes in the Antarctic Ice Sheet above its present surface elevation. Questions of
75 ice sheet thickness and ice stream dynamical behaviour therefore rely on glacial

76 geology investigations on nunataks and ice-free ground, but this is difficult as ~99%
77 of the Antarctic continent is glacierised. The Ulu Peninsula, James Ross Island, is
78 one of the largest ice-free areas on the north-east Antarctic Peninsula, and it
79 preserves a detailed record of glacial fluctuations. The aim of this paper is therefore
80 to use cosmogenic isotope exposure-age dating of terrestrial erratic boulders on ice-
81 free land on James Ross Island, north-eastern Antarctic Peninsula, to define the
82 evolution of Last Glacial Maximum (LGM) ice in the Prince Gustav Channel region
83 between Trinity Peninsula and James Ross Island (Fig. 1).

84

85 **STUDY AREA**

86 During the LGM, at ~18 ka, ice draining from the north-eastern Antarctic Peninsula
87 coalesced with the Mount Haddington Ice Cap on James Ross Island (Bentley and
88 Anderson, 1998; Camerlenghi et al., 2001; Evans et al., 2005; Heroy and Anderson,
89 2007; Johnson et al. 2011; Davies et al., 2012a). Isotopic evidence from an ice core
90 on Mount Haddington (see Fig. 1 for location) indicates that it existed as an
91 independent ice dome throughout the LGM, and was not overrun by isotopically
92 colder ice from Trinity Peninsula (Mulvaney et al., 2012). Ice coalesced from the
93 Mount Haddington Ice Cap and accumulation areas on Trinity Peninsula to form a
94 palaeo-ice stream flowing northwards and southwards to the continental shelf edge,
95 with an ice divide in central Prince Gustav Channel. The geological record of Prince
96 Gustav Ice Stream is largely derived from marine sediment cores and swath
97 bathymetry, which reveal subglacial tills and mega-scale glacial lineations in Prince
98 Gustav Channel and Vega Basin (Fig. 1) (Camerlenghi et al., 2001; Evans et al.,
99 2005). The LGM history of the Antarctic Peninsula Ice Sheet and its post-LGM
100 recession is reconstructed here using cosmogenic isotope exposure-age dating of

101 erratic boulders transported by the Antarctic Peninsula Ice Sheet onto James Ross
102 Island (Figs 1 and 2).

103

104 Ulu Peninsula on James Ross Island is largely ice-free, with several small glaciers
105 and ice domes on flat-topped volcanic mesas. It is uniquely placed to provide a
106 terrestrial record of the dynamics of the LGM ice sheet because Trinity Peninsula
107 and James Ross Island are geologically distinct (Fig. 1). The Antarctic Peninsula is
108 dominated by Permo-Triassic metamorphic rocks of the Trinity Peninsula Group, into
109 which are intruded granitic rocks (Aitkenhead, 1975; Smellie et al., 1996). James
110 Ross Island is formed entirely of Cretaceous sedimentary rocks and unconsolidated
111 sediments, overlain by the cliff-forming Neogene basaltic James Ross Island
112 Volcanic Group, with glacial strata (diamictites) at the base and within (Pirrie et
113 al., 1997; Hambrey and Smellie, 2006; Hambrey et al., 2008; Smellie et al., 2008,
114 2013). Lavas in the James Ross Island Volcanic Group are flood basalts associated
115 with hyaloclastite deltas that together form flat-topped mesas above the Cretaceous
116 strata (Nelson, 1975; Nývlt et al., 2011; Smellie et al., 2013). Granitic and
117 metamorphic erratic boulders from Trinity Peninsula (Bibby, 1966; Nelson et al.,
118 2009; Riley et al., 2011) record incursions of Trinity Peninsula ice onto James Ross
119 Island (Hambrey and Smellie, 2006; Hambrey et al., 2008; Johnson et al., 2011; Fig.
120 2).

121

122 Climatic records indicate that the region has been warming since the 1930s
123 (Vaughan et al. 2003), although ice-core records suggest that warming began 600
124 years ago (Mulvaney et al. 2012), with summer snow-melt accelerating during the
125 twentieth century (Abram et al. 2013). This warming has been associated with

126 changes in the westerly winds around Antarctica, which produce warming over the
127 Antarctic Peninsula. Most land-terminating glaciers on Ulu Peninsula are receding
128 (Carrivick et al., 2012; Davies et al., 2012b; Engel et al., 2012), with up to 100 m of
129 recession since their most recent readvance. These glaciers are surrounded by
130 prominent ice-cored moraines (Carrivick et al., 2012; Davies et al., 2013). More
131 widely, tidewater glaciers around the northern Antarctic Peninsula are also shrinking
132 in response to continued atmospheric warming (Davies et al. 2012b), which also
133 resulted in the collapse of Prince Gustav Ice Shelf in 1995 (Skvarca et al. 1995;
134 Cooper, 1997).

135

136

137 **METHODS**

138 **Cosmogenic nuclide exposure-age dating**

139 ***Sampling strategy***

140 Cosmogenic isotope dating of glacially transported and erratic boulders is now a
141 widely accepted method for dating glacial landforms such as moraines, where it
142 is possible to use crest-line boulders to establish the age of moraine formation
143 (Gosse and Phillips, 2001; Cockburn and Summerfield, 2004; Balco, 2011;
144 Applegate et al., 2012). It is particularly useful in Antarctica, where there are few
145 terrestrial organic remains and the large marine-reservoir effect makes conventional
146 radiocarbon dating difficult (Ingólfsson, 2004; Davies et al., 2012a). The high winds
147 and arid climate reduce the probability of perpetual burial by drifting snow or
148 sediment (Bentley et al., 2006; Mackintosh et al., 2007). However, Antarctic glaciers
149 are frequently cold-based or polythermal, and may be frozen to their beds. Glacially
150 transported boulders and overridden bedrock surfaces may therefore suffer little

151 erosion, and thus retain an inherited cosmogenic nuclide signal. Additionally, in the
152 study area on James Ross Island, granite erratics may be reworked from much older
153 Neogene diamictites (Nývlt et al., 2011). We therefore collected and analysed
154 granitic samples for both ^{26}Al and ^{10}Be and show our results on plots of $^{26}\text{Al}/^{10}\text{Be}$
155 versus ^{10}Be to discriminate samples that may be reworked from Neogene diamictites
156 (cf. Bentley et al., 2006; Wilson et al., 2008).

157

158 Samples were collected following the guidelines of Gosse and Phillips (2001) and
159 Balco (2011). We sampled boulders with a *b*-axis >1.0 m wherever possible (Tables
160 1 and 2; Figure 3) because using larger boulders reduces the possibility of burial or
161 exhumation during periglacial recycling of clasts within the active layer. Larger
162 boulders standing proud on the land surface are also likely to be wind-scoured and
163 therefore clear of snow during the winter. Only boulders on stable moraine crests
164 were sampled, avoiding boulders on uneven or unstable surfaces, which may have
165 moved since deposition. Samples were collected only from the upper surfaces of the
166 boulders using a hammer and chisel, and all samples were less than 5 cm thick
167 (considerably less for many of the granite boulders, which generally produced >1 cm
168 thick surface flakes when sampled). Detailed site descriptions (e.g.
169 geomorphological context, surrounding sediment texture, boulder dimensions,
170 weathering characteristics) were made for each sample. Sample locations were
171 recorded using a hand-held GPS, accurate to ± 5 m in the horizontal dimension.
172 Skyline measurements were collected with a compass-clinometer at all sites to
173 check for possible topographic shielding (i.e. to check if the angle to the horizon was
174 greater than 20°). To avoid complexities associated with possible marine inundation
175 and recent iceberg transportation, all boulders were collected from sites above 30

176 metres above sea level (m a.s.l.), the highest regional Holocene marine level (Hjort
177 et al., 1997; Fretwell et al., 2010).

178

179 ***Chemical analysis***

180 The granite boulders yielded quartz, which was analysed with ^{10}Be and ^{26}Al , and
181 basalt boulders were crushed and the whole-rock chemistry was analysed for ^{36}Cl .
182 The sample preparation and $^{10}\text{Be}/^{26}\text{Al}$ measurement procedures followed standard
183 protocols (Wilson et al., 2008; Glasser et al., 2009; Ballantyne et al., 2009). We
184 added 250 μg Be to each sample as a carrier. Inherent Al concentrations in quartz
185 were determined with an ICP-OES at the Scottish Universities Environmental
186 Research Centre (SUERC). An aluminium carrier was added to most samples so
187 that 2 mg Al per sample was reached.

188

189 The ^{10}Be and ^{26}Al exposure ages and internal uncertainties (Tables 1 and 2) were
190 calculated with the CRONUS-earth online calculators version 2.2
191 (<http://hess.ess.washington.edu/math/>; Wrapper script: 2.2; Main calculator: 2.1;
192 Objective function: 2; Constants: 2.2.1; Muons: 1.1; see Balco et al. 2008). Because
193 production rates vary globally, Table 3 provides ^{10}Be and ^{26}Al ages calculated using
194 the mid-latitude southern hemisphere New Zealand calibration dataset for reference
195 and completeness (Putnam et al., 2010).

196

197 Samples for ^{36}Cl analysis were crushed, sieved to 125–250 μm , enriched in
198 pyroxene by magnetic separation, and leached in hot 2 M HNO_3 to remove meteoric
199 ^{36}Cl contamination. Each sample was then split into two fractions: c. 2 g for
200 elemental analysis and c. 20 g for analysis of ^{36}Cl with accelerator mass

201 spectrometry (AMS). ICP-OES and ICP-MS measurements were used to determine
202 the Ca, K, Ti, Fe, U, Th and REE contents. Chlorine was extracted and purified to
203 produce AgCl for AMS analysis according to the procedures described in Vincent et
204 al. (2010). A high $^{35}\text{Cl}/^{37}\text{Cl}$ carrier was used to determine the total Cl concentration by
205 AMS Isotope Dilution technique (AMS-ID; Di Nicola et al., 2009).

206

207 ^{36}Cl exposure ages and internal uncertainties were calculated according to
208 Schimmelpfennig et al. (2009). Sea level-high latitude ^{36}Cl production rates of
209 48.8 ± 3.4 , 162 ± 25 , 13 ± 3 and 1.9 ± 0.2 atoms $^{36}\text{Cl g}^{-1} \text{ a}^{-1}$, from Ca, K, Ti and Fe
210 respectively, were used (Schimmelpfennig et al., 2009) and scaled according to the
211 Stone (2000) scaling scheme. The time-independent Lal/Stone scheme was chosen
212 to be consistent with calculated ^{36}Cl ages and other ages published for the Antarctic
213 Peninsula (Bentley et al., 2006; Davies et al., 2012a).

214

215 ***Calculation of uncertainties***

216 Primary Standards NIST-SRM4325, PRIME-Z92-0222 and PRIME-Z93-0005, with
217 nominal ratios $2.79\text{E-}11$ $^{10}\text{Be}/\text{Be}$, $4.11\text{E-}11$ $^{26}\text{Al}/\text{Al}$ and $1.2\text{E-}12$ $^{36}\text{Cl}/\text{Cl}$, were used for
218 the AMS measurements (Freemnan et al., 2004). These agree with those prepared
219 by Nishiizumi *et al.* (2007), which were used as secondary standards. The reported
220 uncertainties of the cosmonuclide concentrations include 2.5% for the AMS and
221 chemical preparation. Blank corrections ranged between 4 and 11% for $^{10}\text{Be}/\text{Be}$
222 ratios; between 0.1 and 3.2% for $^{26}\text{Al}/\text{Al}$ ratios; and between 5 and 7% for $^{36}\text{Cl}/\text{Cl}$
223 ratios. These corrections are included in the stated uncertainties.

224

225 **RESULTS: GLACIAL GEOLOGY AND GEOMORPHOLOGY**

226 Ulu Peninsula is characterised by several small cirque and valley glaciers, with ice
227 domes on flat-topped volcanic mesas (Figs. 2, 3A, 3B). On the tops of the mesas
228 (above 370 m a.s.l.), the flood basalts and hyaloclastite deltas have been broken
229 down to form blockfields where periglacial action is evident. Rare isolated granite
230 boulders occur in these locations (Fig 3B). The interior of Ulu Peninsula is widely
231 mantled by an erratic-poor, basaltic pebble-cobble gravel. Subangular pebbles and
232 cobbles form a lag on the surface, with frequent basalt and rare granitic boulders.
233 This surface has been deflated, and fine to coarse sand is present beneath the
234 pebble lag (Fig. 3E). There is evidence of localised stone-sorting by periglacial
235 processes in these areas (Davies et al., 2013).

236

237 Coastal areas, both to the west and east of Ulu Peninsula, are commonly
238 characterised by glacial deposits with far higher proportions of Trinity Peninsula
239 erratic material, and with many more large granite boulders. Some of this drift is
240 associated with moraine fragments (for example at Kaa Bluff and St Martha Cove;
241 Figs. 2, 3C, 3D). Large (up to 2 m *b*-axis) Trinity Peninsula granite boulders and sub-
242 rounded, striated, faceted, glacially transported, locally derived boulders are
243 scattered widely across the surface of Ulu Peninsula (Fig. 2). Together with
244 streamlined bedrock ridges, smoothed and sculpted cols and passes, the glacial
245 drifts indicate that the area was inundated by the Antarctic Peninsula Ice Sheet.

246

247 **RESULTS: COSMOGENIC ISOTOPE DATING**

248 Cosmogenic ^{26}Al and ^{10}Be data from granite erratic boulders and ^{36}Cl from locally
249 derived glacially transported basalt boulders on James Ross Island indicate the
250 timing and duration of deglacial ice-streaming events (Figs. 2, 4; Tables 1 and 2).

251 The $^{26}\text{Al}/^{10}\text{Be}$ ratios of all granite samples were statistically equal to or greater than
252 the production rate ratio (Fig. 5), suggesting that they have been constantly exposed
253 and not subjected to repeated burial and exhumation, which may be an issue in cold
254 Antarctic environments (Bentley et al., 2006) and where there is the potential for
255 reworking of older Neogene glacial deposits (Nývlt et al., 2011). Boulder ages are
256 presented as a weighted mean of the ^{26}Al and ^{10}Be ages (Wilson et al., 2008).
257 Following the convention in Antarctica, we use the oldest age in cases where there is
258 geological scatter in the sample ages because boulders may slip downslope, rotate,
259 or be shielded by snow (Balco et al., 2011). This method is appropriate because the
260 co-isotope plot suggests that inheritance is not a problem in the samples.

261

262 Two large white granite boulders embedded on the summit of Lachman mesa at 370
263 metres above sea level (JRI49 and JRI50; Figs. 2, 4; Table 1) yielded cosmogenic
264 isotope ages of 17.7 ± 0.8 and 15.1 ± 0.4 . Near Davies Dome, basalt samples JRI33
265 and JRI34 yield ^{36}Cl ages of 19.9 ± 7.2 and 22.1 ± 6.6 ka (Fig. 2). These ages
266 indicate that the age of deglaciation of Lachman mesa is ~ 18 ka, synchronous with
267 the observed ice-sheet recession across the continental shelf (Heroy and Anderson,
268 2005; 2007). Somewhat younger deglaciation ages of 11.8 and 13.8 ka were
269 obtained for basalt bedrock at Crisscross Crags and Patalamon Mesa (Figure 1), at
270 c. 600 m elevation, by Johnson et al. (2009). However, the younger ages probably
271 relate to the persistence of local ice domes (both localities sustain ice domes today)
272 that took longer to decay and expose bedrock than at Lachman mesa.

273

274 In the most northerly part of Ulu Peninsula, a lower elevation sample (JRI35) in the
275 granite-rich drift (45 m.a.s.l.) on Cape Lachman on the NW of James Ross Island,

276 provides an exposure age of 6.3 ± 0.2 ka. South of Brandy Bay, samples JRI01 and
277 JRI03, which are large granite erratic boulders in the coastal erratic-rich drift at
278 elevations of ~ 100 m.a.s.l. on “San Carlos Hill”, south of San Carlos Point (Fig. 2),
279 provide exposure ages of 12.2 ± 0.4 and 11.3 ± 0.4 ka respectively. A large granite
280 erratic boulder in Sharp Valley, NW of James Ross Island (JRI09), provides a
281 cosmogenic isotope age of 8.9 ± 0.2 ka. Further west, sample JRI 62 collected at
282 Kaa Bluff at 144 m.a.s.l. (Figs. 3C, 4), NW James Ross Island, indicates that
283 Peninsula ice receded from James Ross Island around 7.6 ± 0.3 ka. In the interior of
284 Ulu Peninsula, sample JRI26 is an isolated granite boulder, located on a basalt drift
285 at San Jose Pass, which indicates ice recession at 6.7 ± 0.3 ka. On the eastern side
286 of the island, a granite erratic boulder in granite-rich drift on a subdued, degraded
287 moraine ridge (sample JRI29 at St. Martha Cove, Fig. 2) was dated to 6.1 ± 0.3 ka.

288

289 **DISCUSSION: IMPLICATIONS FOR THE LAST GLACIAL MAXIMUM ANTARCTIC** 290 **ICE SHEET**

291 The location of the erratic boulders and their exposure ages indicate that at ~ 18 ka, a
292 relatively thick Antarctic Peninsula Ice Sheet deposited erratic boulders derived from
293 Trinity Peninsula at elevations of up to ~ 370 m a.s.l. on James Ross Island (our
294 data) and on Seymour Island (Johnson et al., 2011). Subsequent surface-lowering of
295 the LGM ice sheet is indicated by the younger exposure ages at lower elevations.
296 This surface-lowering marks a dynamical change coincident with the onset of the
297 LGM Prince Gustav Ice Stream. This dynamical change occurred after ~ 18 ka but
298 before 12.2 ± 0.4 ka, which is the exposure age of the oldest erratic boulder (JRI01)
299 in the coastal erratic-rich drift of the Ulu Peninsula (Fig. 2). The coastal erratic-rich
300 drift is interpreted as demarking a region of enhanced wet-based glacial deposition

301 (Davies et al., 2013), which, combined with the offshore lineations mapped in Vega
302 Basin (Evans et al., 2005; Camerlenghi et al., 2001; Fig. 2) is interpreted as the
303 lateral margin of the Prince Gustav Ice Stream. Sample JRI62 is located on a
304 moraine fragment on Kaa Bluff at 144 m.a.s.l., and this location effectively delimits
305 the maximum height of the lateral margins of the Prince Gustav Ice Stream. The ice
306 surface therefore lowered at least 230 m during the interval 18 to 12.2 ka. Younger
307 ages for granite erratic boulders occupying low-lying coastal sites on western Ulu
308 Peninsula indicate that the ice stream continued to impinge on the shores of James
309 Ross Island until ~7 ka. Local ice from Mount Haddington Ice Cap remained on Ulu
310 Peninsula, flowing east out of St. Martha Cove until 6.1 ± 0.3 ka. An ice-sheet
311 configuration similar to that of today was achieved after ~6 ka.

312

313 These data are supported by field observations and cosmogenic-nuclide exposure
314 ages from ice-free areas adjacent to the Sjögren, Boydell, and Drygalski Glaciers on
315 the north-eastern Antarctic Peninsula (Fig. 1), where the LGM ice-surface elevation
316 near the present coastline was ~500 m a.s.l., with cold-based ice at elevations above
317 100-150 m a.s.l., and wet-based ice below (Balco et al., 2013). The ice-surface
318 elevation decreased from ~500 m a.s.l. to near present-day sea-level between 9 ka
319 and ~4 ka, confirming previous interpretations that deglaciation took place between
320 >14 ka and ~6 ka (Ingólfsson et al., 2003). The minimum age for deglaciation in
321 Prince Gustav Channel is 10.6 cal. ka BP, following a period of rapid warming
322 recorded in the James Ross Island ice core (Figs. 1 and 6; Mulvaney et al., 2012).
323 These data confirm our estimate of 144 m a.s.l. for the Prince Gustav Ice Stream at
324 7.6 ± 0.3 ka and complete withdrawal of the ice stream from Ulu Peninsula by ~6 ka.
325 Radiocarbon ages from glaciomarine sediments in southern Prince Gustav Channel

326 (Fig. 1) indicate ice-free conditions here by ~9 cal. ka BP (Pudsey and Evans, 2001).
327 Published exposure ages Johnson Mesa (260-304 m a.s.l.) and Terrapin Hill (80-85
328 m a.s.l.) from James Ross Island (Fig. 1) also indicate the recession of Prince
329 Gustav Ice Stream and imply deglaciation in Prince Gustav Channel around 6-8 ka
330 (Johnson et al., 2011).

331

332 Deglaciation in early Holocene time is also indicated by the relative sea-level record
333 at Beak Island, north of Ulu Peninsula (Figs. 1, 6), which became ice-free with the
334 onset of glaciomarine sedimentation at 10.7 cal. ka BP (Roberts et al., 2011). A sea
335 level high-stand at 8 cal. ka BP indicates rapid eustatic sea-level rise, which
336 outpaced isostatic readjustment at this time. The Beak Island sea-level record
337 agrees with other published sea-level data in this region (Hjort et al., 1997) and with
338 isostatically coupled sea-level models (Huybrechts, 2002; Peltier, 1998). These
339 relative sea-level data confirm the interpretation of rapid ice-stream thinning,
340 recession and drawdown during a period of rapid warming in the early Holocene
341 Epoch (cf. Mulvaney et al., 2012; Fig. 6).

342

343 On the western Antarctic Peninsula, oxygen isotope data from diatoms in marine
344 sediment cores in the Palmer Deep indicate that the period from 13.0-12.1 ka was
345 characterised by rapid deglaciation, coincident with ice-stream retreat in the outer
346 and inner Anvers Trough, the breakup of Marguerite Bay ice shelf and decreases in
347 sea ice in Maxwell Bay (Pike et al., 2013). Our study shows that by 12 ka, the Prince
348 Gustav Ice Stream on the eastern Antarctic Peninsula was already thinning and
349 receding, suggesting that ice-stream response was coincident on both the western
350 and eastern Antarctic Peninsula. This region-wide glacier recession has been linked

351 to increased upwelling of upper Circumpolar Deep Water onto the continental shelf,
352 associated with strong winds in the Southern Ocean westerlies (Pike et al., 2013).
353 After 12 ka, a slow-down in glacial recession is noted by decreased glacial discharge
354 both in the Palmer Deep (Pike et al., 2013), and in the slower recession of Prince
355 Gustav Ice Stream around Ulu Peninsula. The final recession of Prince Gustav Ice
356 Stream around 7.6 ka is also coincident with increased upwelling of Circumpolar
357 Deep Water.

358

359 These changes in the upwelling of Circumpolar Deep Water have been related to
360 variations in ENSO as well as the Southern Annular Mode (Pike et al., 2013), and
361 recent increases in summer melt on James Ross Island have also been related to a
362 strengthening of the Southern Annular Mode (Abram et al., 2013). Our new data on
363 previous ice-stream response to past climatic variations confirm that the north-
364 eastern Antarctic Peninsula is a dynamic environment, sensitive to small changes in
365 oceanic and atmospheric circulation. This has important implications for future ice
366 dynamics as global atmospheric temperatures approach those of the mid-Holocene
367 climatic optimum (Marcott et al., 2013).

368

369 **CONCLUSIONS**

370

371 Cosmogenic isotope dating of granite and basalt erratic boulders indicates a three-
372 phase LGM ice-sheet evolution on James Ross Island (Fig. 6). Firstly, until ~18 ka
373 James Ross Island was inundated by a thick Antarctic Peninsula Ice Sheet. An
374 important change occurred after ~18 ka when the ice sheet became more dynamic.
375 The development of the Prince Gustav Ice Stream resulted in lowering of the

376 regional ice-sheet surface. Secondly, ice-sheet thinning and the onset of Prince
377 Gustav Ice Stream from 18-12 ka coincided with rapid eustatic sea-level rise
378 (Roberts et al., 2011) and rapidly increasing air temperatures recorded in the Mount
379 Haddington ice cores (Fig. 1; Mulvaney et al., 2012). Finally, after ~8 ka, rapid
380 isostatic uplift produced falling relative sea level, coincident with ice-stream
381 recession and deglaciation of Ulu Peninsula. By 6 ka, ice sheet configuration was
382 similar to present. We conclude that ice streams exerted a strong control on the
383 deglaciation of the LGM Antarctic Peninsula Ice Sheet. Although deglacial ice-stream
384 initiation has been inferred for former mid-latitude ice sheets, this is the first robustly
385 dated example of Antarctic ice-stream initiation, duration and thinning.

386

387 **ACKNOWLEDGEMENTS**

388 This work was funded by the UK Natural Environment Research Council (NERC)
389 under the Antarctic Funding Initiative NE/F012942/1). Transport, logistics and
390 fieldwork on James Ross Island were supported by the British Antarctic Survey, and
391 we thank the captain and crew of the *RRS Ernest Shackleton* and the *RRS James*
392 *Clark Ross* for their support. We thank Alan Hill for his field logistical support. ^{10}Be ,
393 ^{26}Al and ^{36}Cl analyses were supported by a NERC CIAF grant (9035/0407), and we
394 also acknowledge Joyce Wilcox and Allan Davidson (both SUERC) for help with
395 these analyses.

396

397 **FIGURE CAPTIONS**

398 Figure 1. Geographical and geological context of James Ross Island and Trinity
399 Peninsula, with bathymetric data (50 m resolution). Inset shows wider location of
400 James Ross Island. Previously published ages are from Hjort et al. (1997), Pudsey

401 and Evans (2001), Heroy and Anderson (2005; 2007), Johnson et al. (2009, 2011)
402 and Balco et al. (2013). Circles are calibrated radiocarbon ages (ka BP) and
403 diamonds are ^{10}Be cosmogenic nuclide exposure ages (ka). Mega-scale glacial
404 lineations are shown in Prince Gustav Channel. JRIVG = James Ross Island
405 Volcanic Group. Location of Fig. 2 is indicated.

406

407 Figure 2. Geomorphological map of Ulu Peninsula showing sample location and ID
408 with cosmogenic nuclide ages in bold (green stars and triangles). Ages are in ka.
409 The coastal 'erratic-rich drift', which denotes the lateral margins of Prince Gustav Ice
410 Stream, is indicated by cross-hatching. Red circles indicate mapped granite erratic
411 boulders with a b-axis > 1 m. Large, prominent ice-cored moraines occur around
412 modern cirque glaciers, and a large moraine flanks Brandy Bay. Degraded ridges,
413 interpreted as moraine fragments, occur at Kaa Bluff and St. Martha Cove.
414 Previously published cosmogenic nuclide exposure ages are shown. Spot heights
415 are given in metres above sea level (in italics).

416

417 Figure 3. A) Ulu Peninsula from Johnson Mesa. Note the flat-topped volcanic mesas
418 with small ice domes, small cirque glaciers and smooth terrain. B) Cosmogenic
419 nuclide samples JRI 49 on Lachman mesa. An isolated granite boulder on a volcanic
420 blockfield. C) Moraine below Kaa Bluff, with a distinct ridge with numerous white
421 granite boulders and cobbles. Sample JRI 62 in the foreground. D) Cape Lachman,
422 northern promontory on James Ross Island. Numerous granite boulders are present
423 in the saddle at the neck of the promontory. E) Looking down towards the Abernethy
424 Flats, with a boulder-train of Holocene age in the foreground and rare granite
425 boulders.

426

427 Figure 4. James Ross Island boulder samples, showing context and age (ka). The
428 first four boulders are situated at high elevations on mesa surfaces. Samples JRI26
429 and JRI29 are situated in San Jose Pass and St. Martha Cove respectively, and
430 document the recession of ice across the interior of the Ulu Peninsula. The
431 remaining samples are from erratic-rich drifts deposited by the Prince Gustav Ice
432 Stream, which receded in a south-westerly direction from Cape Lachman (12 - 13
433 ka) to San Carlos Hill (~12 ka) and back towards Kaa Bluff (~7 ka).

434

435 Figure 5. Co-isotope plot of $^{26}\text{Al}/^{10}\text{Be}$ versus ^{10}Be . Theoretical cosmogenic
436 concentrations in a surface affected by no erosion and in a surface in erosion
437 equilibrium are depicted by black lines according to CRONUS production rates.
438 External uncertainties of these lines as a result of a 6% error in both ^{10}Be and ^{26}Al
439 production rates are represented by the grey areas. No samples plot in the zone of
440 complex exposure, indicating that the samples have not been buried for a substantial
441 period of time and then exhumed.

442

443 Figure 6. A) Local temperature changes from the Mount Haddington ice core (see
444 Fig. 1 for location) (Mulvaney et al., 2012). Temperature anomaly compared with
445 1961-1990 mean; 100-year average. B) Relative sea level (RSL) curve for Beak
446 Island, Prince Gustav Channel (Fig. 1; Roberts et al., 2011) and a suite of coupled
447 sea-level models (Peltier, 1998; Huybrechts, 2002), and marine microfossils from
448 James Ross Island (Ingólfsson et al., 1992; Hjort et al., 1997). C) Sample altitude
449 and mean age showing ice-sheet thinning, and the cluster of ^{10}Be ages related to the
450 recession of Prince Gustav Ice Stream (this study). Triangles indicate granite

451 boulders on basalt-rich lag surfaces at high elevations (>360 m a.s.l.) (4 samples)
452 deposited by a thick, cold Antarctic Peninsula Ice Sheet. Diamonds indicate Trinity
453 Peninsula erratic boulders on coastal areas of James Ross Island within the erratic-
454 rich drift (5 samples), deposited by Prince Gustav Ice Stream. Squares (2 samples)
455 indicate lower elevation samples deposited by the thinning ice sheet in the interior of
456 Ulu Peninsula. The period of rapid ice-sheet thinning and onset of Prince Gustav Ice
457 Stream observed on Ulu Peninsula coincides with rapid regional temperature
458 increases and rapid eustatic sea-level rise; the youngest deglaciation ages coincide
459 with a period of rapid isostatic uplift on nearby Beak Island (Fig. 1; Roberts et al.,
460 2011).

461

462 **TABLE CAPTIONS**

463 Table 1. Sample details used to calculate ^{10}Be ages in the Cronus-earth online
464 calculators (Balco et al. 2008).

465

466

467 Table 2. Summary of new cosmogenic nuclide ages from Ulu Peninsula. The ^{10}Be
468 ages are presented in the text and figures because the $^{26}\text{Al}/^{10}\text{Be}$ ratios are
469 statistically equal or greater than the production ratio, suggesting no complex
470 exposure or burial history. JRI = James Ross Island, APIS = Antarctic Peninsula Ice
471 Sheet.

472

473

474 Table 3. Calculations of ^{10}Be ages using the Cronus-earth online calculator (Balco et
475 al. 2008) with the New Zealand-Macaulay calibration dataset (Putnam et al., 2010)
476 and the global time-independent Lal/Stone scheme. There is a difference of ~16%
477 between the ages when calculated using these different production rates.

478

479 REFERENCES

- 480 Abram, N.J., Mulvaney, R., Wolff, E.W., Triest, J., Kipfstuhl, S., Trusel, L.D., Vimeuz,
481 F., Fleet, L. and Arrowsmith, C. 2013. Acceleration of snowmelt in an Antarctic
482 Peninsula ice core during the twentieth century. *Nature Geoscience*
483 doi:10.1038/ngeo1787.
- 484 Aitkenhead, N., 1975. The geology of the Duse Bay—Larsen Inlet area, north-east
485 Graham Land (with particular reference to the Trinity Peninsula Series). *British*
486 *Antarctic Survey Scientific Reports* 51, 1-62.
- 487 Applegate, P. J., Urban, N. M, Keller, K., Lowell, T. V., Laabs, B. J. C., Kelly, M. A.,
488 and Alley, R. B., 2012. Improved moraine age interpretations through explicit
489 matching of geomorphic process models to cosmogenic nuclide measurements
490 from single landforms. *Quaternary Research* 77, 293-304.
- 491 Balco, G.A. 2011. Contributions and unrealized potential contributions of
492 cosmogenic-nuclide exposure dating to glacier chronology, 1990-2010.
493 *Quaternary Science Reviews* 30, 3-27.
- 494 Balco, G.A., Schaefer, J.M. and LARISSA Group. 2013. Exposure-age record of
495 Holocene ice sheet and ice-shelf change in the northeast Antarctic Peninsula.
496 *Quaternary Science Reviews* 59, 101-111.

497 Ballantyne, C.K., Schnabel, C. and Xu, S. 2009. Exposure dating and
498 reinterpretation of coarse debris accumulations ('rock glaciers') in the Cairngorm
499 Mountains, Scotland. *Journal of Quaternary Science* 24, 19-31.

500 Barrand, N. E., Vaughan, D. G., Steiner, N., Tedesco, M., Kuipers Munneke, P., van
501 den Broeke, M. R., and Hosking, J. S. (2013). Trends in Antarctic Peninsula
502 surface melting conditions from observations and regional climate modeling.
503 *Journal of Geophysical Research: Earth Surface* **118** (1), 315-330.

504 Bentley, M.J. and Anderson, J.B., 1998. Glacial and marine geological evidence for
505 the ice sheet configuration in the Weddell Sea-Antarctic Peninsula region during
506 the Last Glacial Maximum. *Antarctic Science* 10, 309-325.

507 Bentley, M.J., Fogwill, C.J., Kubik, P.W. and Sugden, D.E. 2006, Geomorphological
508 evidence and cosmogenic $^{10}\text{Be}/^{26}\text{Al}$ exposure ages for the Last Glacial Maximum
509 and deglaciation of the Antarctic Peninsula Ice Sheet. *Geological Society of*
510 *America Bulletin* 118, 1149-1159.

511 Bibby, J.S., 1966, *The stratigraphy of part of north-east Graham Land and the James*
512 *Ross Island Group*, 37 British Antarctic Survey, London.

513 Bintanja, R., van Oldenborgh, G.J., Drijfhout, S.S., Wouters, B. and Katsman, C.A.
514 2013, Important role for ocean warming and increased ice-shelf melt in Antarctic
515 sea-ice expansion. *Nature Geoscience* 6, 376-379.

516 Camerlenghi, A., Domack, E., Rebesco, M., Gilbert, R., Ishman, S., Leventer, A.,
517 Brachfeld, S. and Drake, A., 2001. Glacial morphology and post-glacial contourites
518 in northern Prince Gustav Channel (NW Weddell Sea, Antarctica). *Marine*
519 *Geophysical Researches* 22, 417-443.

520 Carrivick, J.L., Davies, B.J., Glasser, N.F. and Nývlt, D. 2012. Late Holocene
521 changes in character and behaviour of land-terminating glaciers on James Ross
522 Island, Antarctica. *Journal of Glaciology* 58, 1476-1490.

523 Cockburn, H.A.P. and Summerfield, M.A. 2004. Geomorphological applications of
524 cosmogenic isotope analysis. *Progress in Physical Geography* 28, 1-42.

525 Cook, A.J., Fox, A.J., Vaughan, D.G. and Ferrigno, J.G., 2005. Retreating glacier
526 fronts on the Antarctic Peninsula over the past half-century. *Science* 308 (5721),
527 541-544.

528 Cook, A.J. and Vaughan, D.G., 2010. Overview of areal changes of the ice shelves
529 on the Antarctic Peninsula over the past 50 years. *The Cryosphere* 4, 77-98.

530 Cooper, A.P.R., 1997. Historical observations of Prince Gustav Ice Shelf. *Polar*
531 *Record* 33, 285-294.

532 Davies, B.J., Hambrey, M.J., Smellie, J.L., Carrivick, J.L. and Glasser, N.F. 2012a.
533 Antarctic Peninsula Ice Sheet evolution during the Cenozoic Era. *Quaternary*
534 *Science Reviews* 31, 30-66.

535 Davies, B.J., Carrivick, J.L., Glasser, N.F., Hambrey, M.J. and Smellie, J.L. 2012b.
536 Variable glacier response to atmospheric warming, northern Antarctic Peninsula,
537 198802009. *The Cryosphere* 6, 1031-1048.

538 Davies, B.J., Glasser, N.F., Carrivick, J.L., Hambrey, M.J., Smellie, J.L. and Nývlt, D.
539 2013. Landscape evolution and ice-sheet behaviour in a semi-arid polar
540 environment: James Ross Island, NE Antarctic Peninsula. in *Antarctic*
541 *Palaeoenvironments and Earth Surface Processes*, Vol. 381 (eds. Hambrey, M.J.,
542 Barker, P.F., Barrett, P.J., Bowman, V.C., Davies, B.J., Smellie, J.L. and Tranter,
543 M.) Geological Society of London, Special Publications, London.

544 Di Nicola, L, Schnabel, C, Wilcken, KM, and Gméling, K 2009. Determination of
545 chlorine concentrations in whole rock samples with prompt-gamma activation
546 analysis (PGAA) and isotope dilution AMS. *Quaternary Geochronology* 4, 501-
547 507.

548 Engel, Z., Nývlt, D., and Láska, K., 2012. Ice thickness, areal and volumetric
549 changes of Davies Dome and Whisky Glacier (James Ross Island, Antarctic
550 Peninsula) in 1979-2006. *Journal of Glaciology* 58, 904-914.

551 Evans, J., Pudsey, C.J., Ó Cofaigh, C., Morris, P. and Domack, E. 2005. Late
552 Quaternary glacial history, flow dynamics and sedimentation along the eastern
553 margin of the Antarctic Peninsula Ice Sheet. *Quaternary Science Reviews* 24,
554 741-774.

555 Freeman, S., Xu, S., Schnabel, C., Dougans, A., Tait, A., Kitchen, R., Klody, G.,
556 Loger, R., Pollock, T., Schroeder, J., Sundquist, M. 2004. Initial measurements
557 with the SUERC accelerator mass spectrometer. *Nuclear Instruments and*
558 *Methods in Physics Research Section B: Beam Interactions with Materials and*
559 *Atoms*, 223–224, 195 – 198.

560 Fretwell, P.T., Hodgson, D.A., Watcham, E.P., Bentley, M.J. and Roberts, S.J. 2010.
561 Holocene isostatic uplift of the South Shetland Islands, Antarctic Peninsula,
562 modelled from raised beaches. *Quaternary Science Reviews* 29, 1880-1893.

563 Glasser, N.F., Clemmens, S., Schnabel, C., Fenton, C.R. and Mchargue, L. 2009.
564 Tropical glacier fluctuations in the Cordillera Blanca, Peru between 12.5 and 7.6
565 ka from cosmogenic Be-10 dating. *Quaternary Science Reviews* 28, 3448-3458.

566 Gosse, J.C. and Phillips, F.M. 2001. Terrestrial in situ cosmogenic nuclides: theory
567 and application. *Quaternary Science Reviews* 20, 1475-1560.

568 Graham, A.G.C., Larter, R.D., Gohl, K., Hillenbrand, C.-D., Smith, J.A. and Kuhn, G.
569 2009. Bedform signature of a West Antarctic palaeo-ice stream reveals a multi-
570 temporal record of flow and substrate control. *Quaternary Science Reviews* 28,
571 2774-2793.

572 Graham, A.G.C. and Smith, J.A. 2012. Palaeoglaciology of the Alexander Island ice
573 cap, western Antarctic Peninsula, reconstructed from marine geophysical and core
574 data. *Quaternary Science Reviews* 35, 63-81.

575 Gregoire, L.J., Payne, A.J. and Valdes, P.J. 2012. Deglacial rapid sea level rises
576 caused by ice sheet saddle collapses. *Nature* 487, 219-222.

577 Hambrey, M.J. and Smellie, J.L. 2006. Distribution, lithofacies and environmental
578 context of Neogene glacial sequences on James Ross and Vega Islands, Antarctic
579 Peninsula, in Francis, E.A., Pirrie, D. and Crame, J.A., eds, Cretaceous-Tertiary
580 High-Latitude Palaeoenvironments, James Ross Basin, Antarctica, 258, 187-200,
581 Geological Society Special Publication, London).

582 Hambrey, M.J., Smellie, J.L., Nelson, A.E. and Johnson, J.S. 2008. Late Cenozoic
583 glacier-volcano interaction on James Ross Island and adjacent areas, Antarctic
584 Peninsula region. *Geological Society of America Bulletin* 120, 709-731.

585 Heroy, D.C. and Anderson, J.B. 2005. Ice-sheet extent of the Antarctic Peninsula
586 region during the Last Glacial Maximum (LGM) - Insights from glacial
587 geomorphology: *Geological Society of America Bulletin* 117, 1497-1512.

588 Heroy, D.C. and Anderson, J.B. 2007. Radiocarbon constraints on Antarctic
589 Peninsula Ice Sheet retreat following the Last Glacial Maximum (LGM):
590 *Quaternary Science Reviews* 26, 3286-3297.

591 Hjort, C., Ingólfsson, Ó., Möller, P. and Lirio, J.M., 1997. Holocene glacial history and
592 sea-level changes on James Ross Island, Antarctic Peninsula: *Journal of*
593 *Quaternary Science* 12, 259-273.

594 Huybrechts, P. 2002. Sea-level changes at the LGM from ice-dynamic
595 reconstructions of the Greenland and Antarctic ice sheets during the glacial
596 cycles. *Quaternary Science Reviews* 21, 203-231.

597 Ingólfsson, Ó., 2004. Quaternary glacial and climate history of Antarctica. In: J.
598 Ehlers and P.L. Gibbard (Editors), *Quaternary Glaciations - Extent and*
599 *Chronology, Part III*. Developments in Quaternary Science. Elsevier, pp. 3-43.

600 Ingólfsson, Ó., Hjort, C., Björck, S. and Smith, L.R.I. 1992. Late Pleistocene and
601 Holocene glacial history of James Ross Island, Antarctic Peninsula. *Boreas* 21,
602 209-222.

603 Ingólfsson, Ó., Hjort, C. and Humlum, O. 2003. Glacial and climate history of the
604 Antarctic Peninsula since the Last Glacial Maximum: *Arctic, Antarctic and Alpine*
605 *Research* 35, 175-186.

606 Johnson, J.S., Smellie, J.L., Nelson, A.E. and Stuart, F.M. 2009. History of the
607 Antarctic Peninsula Ice Sheet since the early Pliocene—Evidence from
608 cosmogenic dating of Pliocene lavas on James Ross Island, Antarctica. *Global*
609 *and Planetary Change*, 69, 205-213.

610 Johnson, J.S., Bentley, M.J., Roberts, S.J., Binney, S.A. and Freeman, S.P.H.T.
611 2011. Holocene deglacial history of the north east Antarctic Peninsula - a review
612 and new chronological constraints: *Quaternary Science Reviews* 30, 3791-3802.

613 Joughin, I., Tulaczyk, S., Bindschadler, R. and Price, S.F. 2002. Changes in west
614 Antarctic ice stream velocities: Observation and analysis. *J. Geophys. Res.* 107
615 (B11), 2289.

616 Livingstone, S.J., O Cofaigh, C., Stokes, C.R., Hillenbrand, C.-D., Vieli, A. and
617 Jamieson, S.S.R. 2012. Antarctic palaeo-ice streams: *Earth-Science Reviews*
618 111, 90-128.

619 Mackintosh, A., White, D., Fink, D., Gore, D.B., Pickard, J. and Fanning, P.C. 2007.
620 Exposure ages from mountain dipsticks in Mac. Robertson Land, East Antarctica,
621 indicate little change in ice-sheet thickness since the Last Glacial Maximum.
622 *Geology* 35, 551-554.

623 Marcott, S.A., Shakun, J.D., Clark, P.U. and Mix, A.C. 2013. A Reconstruction of
624 Regional and Global Temperature for the Past 11,300 Years. *Science* 339, 1198-
625 1201.

626 Mulvaney, R., Abram, N.J., Hindmarsh, R.C.A., Arrowsmith, C., Fleet, L., Triest, J.,
627 Sime, L.C., Alemany, O. and Foord, S. 2012. Recent Antarctic Peninsula warming
628 relative to Holocene climate and ice-shelf history. *Nature* 489, 141-144.

629 Nelson, P.H.H. 1975. The James Ross Island Volcanic Group of north-east Graham
630 Land. *British Antarctic Survey Scientific Reports* 54, 1-62.

631 Nelson, A.E., Smellie, J.L., Hambrey, M.J., Willaims, M. Vautravers, M., Salzmann,
632 U., McArthur, J.M. and Regelous, M. 2009. Neogene glacial debris flows on
633 James Ross Island, northern Antarctic Peninsula, and their implications for
634 regional climate history. *Quaternary Science Reviews* 28, 3138-3160.

635 Nishiizumi, K., Imamura, M., Caffee, M. W., Southon, J. R., Finkel, R. C., McAninch,
636 J. 2007. Absolute calibration of ^{10}Be AMS standards. *Nuclear Instruments and*
637 *Methods in Physics Research Section B: Beam Interactions with Materials and*
638 *Atoms*, 258, 403 - 413

639 Nývlt, D., Kosler, J., Mlcoch, B., Mixa, P., Bubik, M. and Hendriks, B.W.H. 2011. The
640 Mendel Formation: Evidence for Late Miocene climatic cyclicity at the northern tip

641 of the Antarctic Peninsula. *Palaeogeography Palaeoclimatology Palaeoecology*
642 299, 363-384.

643 Ó Cofaigh, C., Dowdeswell, J.A., Allen, C.S., Hiemstra, J.F., Pudsey, C.J., Evans, J.
644 and Evans, D.J.A., 2005. Flow dynamics and till genesis associated with a
645 marine-based Antarctic palaeo-ice stream. *Quaternary Science Reviews* 24, 709-
646 740.

647 Ó Cofaigh, C., Dowdeswell, J.A., Evans, J. and Larter, R.D., 2008. Geological
648 constraints on Antarctic palaeo-ice-stream retreat. *Earth Surface Processes and*
649 *Landforms* 33, 513-525.

650 Peltier, W.R., 1998. Postglacial variations in the level of the sea: Implications for
651 climate dynamics and solid-Earth geophysics. *Reviews of Geophysics* 36, 603-
652 689.

653 Pike, J., Swann, G.E.A., Leng, M.J. and Snelling, A.M. 2013. Glacial discharge
654 along the west Antarctic Peninsula during the Holocene. *Nature Geoscience* 6,
655 199-202.

656 Pirrie, D., Crame, J. A., Riding, J. B., Butcher, A. R., and Taylor, P. D. 1997. Miocene
657 glaciomarine sedimentation in the northern Antarctic Peninsula region: the
658 stratigraphy and sedimentology of the Hobbs Glacier Formation, James Ross
659 Island. *Geological Magazine* 134, 745-762.

660 Pritchard, H.D., Ligtenberg, S.R.M., Fricker, H.A., Vaughan, D.G., van den Broeke,
661 M.R. and Padman, L. 2012. Antarctic ice-sheet loss driven by basal melting of ice
662 shelves. *Nature* 484, 502-505.

663 Pudsey, C.J. and Evans, J., 2001. First survey of Antarctic sub-ice shelf sediments
664 reveals Mid-Holocene ice shelf retreat. *Geology* 29, 787-790.

665 Putnam, A. E., Schaefer, J. M., Barrell, D. J. A., Vandergoes, M., Denton, G. H.,
666 Kaplan, M. R., Finkel, R. C., Schwartz, R., Goehring, B. M. and Kelley, S. E. 2010.
667 In situ cosmogenic ^{10}Be production-rate calibration from the Southern Alps, New
668 Zealand. *Quaternary Geochronology* 5, 392-409.

669 Riley, T.R., Flowerdew, M.J. and Haselwimmer, C.E., 2011. Geological map of
670 Eastern Graham Land, Antarctic Peninsula (1:625 000 scale), BAS GEOMAP 2
671 Series, Sheet 1 (British Antarctic Survey, Cambridge, UK).

672 Roberts, S.J., Hodgson, D.A., Sterken, M., Whitehouse, P.L., Verleyen, E.,
673 Vyverman, W., Sabbe, K., Balbo, A., Bentley, M.J. and Moreton, S.G., 2011.
674 Geological constraints on glacio-isostatic adjustment models of relative sea-level
675 change during deglaciation of Prince Gustav Channel, Antarctic Peninsula.
676 *Quaternary Science Reviews* 30, 3603-3617.

677 Royles, J., Amesbury, Matthew J., Convey, P., Griffiths, H., Hodgson, Dominic A.,
678 Leng, Melanie J., and Charman, Dan J. (2013). Plants and Soil Microbes Respond
679 to Recent Warming on the Antarctic Peninsula. *Current Biology* 23 (17), 1702-
680 1706.

681 Schimmelpfennig, I., Benedetti, L., Finkel, R., Pik, R., Blard, P.H., Bourles, D.,
682 Burnard, P. and Williams, A. 2009. Sources of *in-situ* ^{36}Cl in basaltic rocks.
683 Implications for calibration of production rates. *Quaternary Geochronology* 4, 441-
684 461.

685 Skvarca, P., Rott, H. and Nagler, T. 1995. Satellite imagery, a base line for glacier
686 variation study on James Ross Island, Antarctica. *Annals of Glaciology* 21, 291-
687 296.

688 Smellie, J.L., Roberts, B., and Hiron, S.R. 1996. Very low- and low-grade
689 metamorphism in the Trinity Peninsula Group (Petmo-Triassic) of northern
690 Graham Land, Antarctic Peninsula. *Geological Magazine* 133, 583-594.

691 Smellie, J.L., Johnson, J.S., McIntosh, W.C., Esser, R., Gudmundsson, M.T.,
692 Hambrey, M.J. and Van Wyk De Vries, B. 2008. Six million years of glacial history
693 recorded in the James Ross Island Volcanic Group, Antarctic Peninsula.
694 *Palaeogeography, Palaeoclimatology, Palaeoecology* 260, 122-148.

695 Smellie, J.L., Johnson, J.S. and Nelson, A.E. 2013. Geological map of James Ross
696 Island. 1. James Ross Island Volcanic Group (1:125 000 scale). BAS GEOMAP 2
697 Series, Sheet 5, British Antarctic Survey, Cambridge, UK.

698 Stone, J.O. 2000. Air pressure and cosmogenic isotope production. *Journal of*
699 *Geophysical Research* 105, 23753–23759.

700 Turner, J., Colwell, S.R., Marshall, G.J., Lachlan-Cope, T.A., Carelton, A.M., Jones,
701 P.D., Lagun, V., Reid, P.A. and Lagovkina, S. 2005. Antarctic climate change
702 during the last 50 years. *International Journal of Climatology* 25, 279-294.

703 Turner, J., Bindshadler, R., Convey, P., di Prisco, G., Fahrback, E., Gutt, J.,
704 Hodgson, D. A., Mayewski, P. A., and Summerhayes, C. P. (2009). *Antarctic*
705 *Climate Change and the Environment*. Scientific Committee on Antarctic
706 Research, Cambridge. 555 pp. Vaughan, D.G., Marshall, G.J., Connelly, W.M.,
707 Parkinson, C., Mulvaney, R., Hodgson, D.A., King, J.C., Pudsey, C.J. and Turner,
708 J. 2003. Recent rapid regional climate warming on the Antarctic Peninsula.
709 *Climatic Change* 60, 243-274.

710 Vincent, P. J., Wilson, P., Lord, T.C., Schnabel, C., Wilcken, K.M. 2010. Cosmogenic
711 isotope (^{36}Cl) surface exposure dating of the Norber erratics, Yorkshire Dales:

712 Further constraints on the timing of the LGM deglaciation in Britain. *Proceedings*
713 *of the Geologists' Association* 121, 24-31.

714

715 Wilson, P., Bentley, M.J., Schnabel, C., Clark, R. and Xu, S. 2008. Stone run (block
716 stream) formation in the Falkland Islands over several cold stages, deduced from
717 cosmogenic isotope (^{10}Be and ^{26}Al) surface exposure dating. *Journal of*
718 *Quaternary Science* 23, 461-473.

719 Winkelmann, R., Levermann, A., Martin, M.A. and Frieler, K. 2012. Increased future
720 ice discharge from Antarctica owing to higher snowfall. *Nature* 492, 239-243.

721

Table

Sample	Date Sampled	Skyline	Lithology	Altitude (m a.s.l.)	Length (m)	Width (m)	Height (m)	Max Sample thickness (cm)	SUERC AMS ID (¹⁰ Be)	¹⁰ Be at/g Qtz	SUERC AMS ID (²⁶ Al)	²⁶ Al at/g Qtz	SUERC AMS ID (³⁶ Cl)	³⁶ Cl at/g rock
JRI 01	22/01/2011	N	Granite	104	1.62	1.28	0.3	3	b5325	76081 ± 2720	a1514	547648 ± 40912	-	-
JRI 03	22/01/2011	N	Granite	103	1.36	1.23	0.63	2	b5326	66821 ± 2759	a1515	564669 ± 28952	-	-
JRI 09	23/01/2011	N	Granite	39	3.6	3.15	1.2	1	b5331	51771 ± 1852	a1519	374483 ± 12691	-	-
JRI 26	29/01/2011	N	Granite	170	1.9	1.3	0.3	1	b5332	43227 ± 2337	a1536	347123 ± 22320	-	-
JRI 29	30/01/2011	N	Granite	25	2.1	1.4	1	2	b5346	35897 ± 2099	a1529	242612 ± 28338	-	-
JRI 33	04/02/2011	N	Basalt	312	1.4	1.2	1	4	-	-	-	-	c2664	213916 ± 76286
JRI 34	04/02/2011	N	Basalt	244	1.7	1.3	0.7	1	-	-	-	-	c2665	258360 ± 75191
JRI 35	06/02/2011	N	Granite	45	3.4	2.1	0.6	1	b5333	36124 ± 1505	a1520	283267 ± 14631	-	-
JRI 49	11/02/2011	N	Granite	360	1.55	0.9	0.55	1	b5348	147849 ± 7181	a1532	897051 ± 121146	-	-
JRI 50	11/02/2011	N	Granite	370	1.55	1.1	0.75	1	b5349	116577 ± 5140	a1533	911094 ± 33796	-	-
JRI 62	20/02/2011	N	Granite	144	0.9	0.65	0.45	1	b5529	47779 ± 1938	a1600	414063 ± 26819	-	-

Table 1

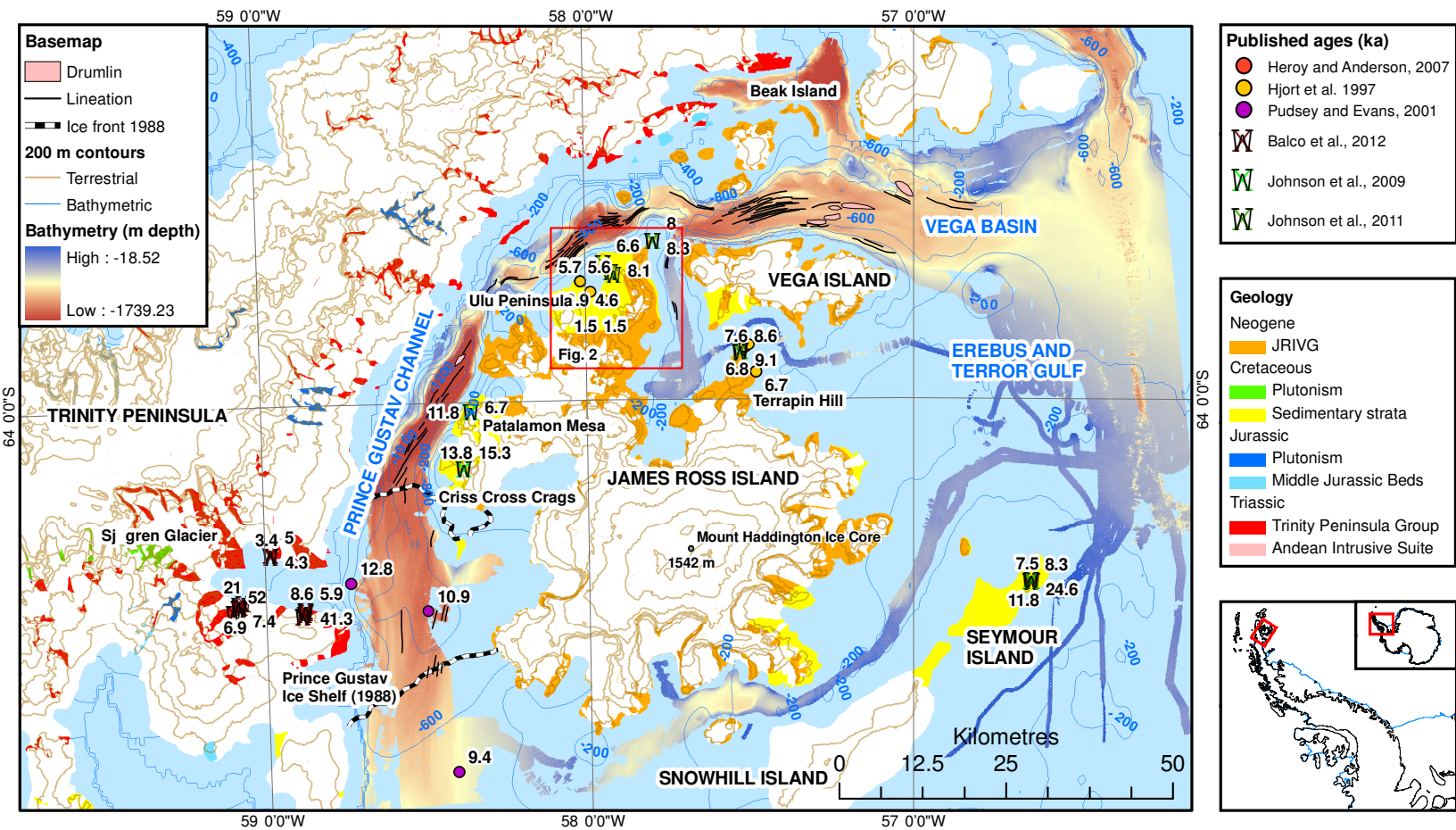
Sample	Elevation (m a.s.l.)	GPS (S)	GPS (W)	Location and context	¹⁰ Be age	²⁶ Al age	²⁶ Al/ ¹⁰ Be	³⁶ Cl age	Considered Age
JRI01	104	63.84267	58.03217	San Carlos Hill; indicates age of incursion of APIS onto NW shore of JRI	12117 ± 435	12873 ± 968	7.2 ± 0.6	-	12244 ± 397
JRI03	103	63.84306	58.03126	San Carlos Hill; indicates age of incursion of APIS onto NW shore of JRI	10566 ± 437	13186 ± 680	8.5 ± 0.6	-	11332 ± 368
JRI09	39	63.85701	58.07312	Sharp Valley; indicates age of incursion of APIS onto NW shore of JRI	8637 ± 312	9264 ± 315	7.2 ± 0.4	-	8948 ± 222
JRI26	170	63.90809	57.89289	San Jose Pass; indicates exposure of interior of JRI	6321 ± 342	7486 ± 483	8.0 ± 0.7	-	6710 ± 279
JRI29	25	63.93596	57.81215	St. Martha Cove; indicates withdrawal of ice from eastern coast of JRI	6159 ± 361	6083 ± 713	6.8 ± 0.9	-	6143 ± 322
JRI33	312	63.90371	58.02856	Large basaltic boulder on drift sheet below Davies Dome; indicates exposure of interior of JRI	-	-	-	19929 ± 7285	19929 ± 7285
JRI34	244	63.90198	58.02380	Large basaltic boulder on drift sheet below Davies Dome; indicates exposure of interior of JRI	-	-	-	22114 ± 6614	22114 ± 6614
JRI35	45	63.80006	57.81549	Cape Lachmann; indicates incursion of APIS ice onto Cape Lachmann. Excluded as it is the youngest boulder in a case of geological scatter	6019 ± 251	6955 ± 360	7.8 ± 0.5	-	6325 ± 206
JRI49	360	63.83208	57.87360	Summit of Lachmann Mesa; indicates age of thick APIS over-riding JRI	17951 ± 876	16096 ± 2191	6.1 ± 0.9	-	17695 ± 813
JRI50	370	63.83592	57.87108	Summit of Lachmann Mesa; indicates age of thick APIS over-riding JRI. Excluded as it is the youngest boulder in a case of geological scatter	14004 ± 620	16192 ± 605	7.0 ± 0.5	-	15125 ± 433
JRI62	144	63.85960	58.10838	Stonely Point-Kaa Bluff; indicates age of incursion of APIS onto NW shore of JRI	7178 ± 292	9178 ± 597	8.7 ± 0.7	-	7564 ± 262

Table 2

Sample	NZ ¹⁰ Be	NZ ²⁶ Al	Global ¹⁰ Be	Global ²⁶ Al
JRI01	14099	14968	12117	12873
JRI03	12293	15332	10566	13186
JRI09	10105	10766	8687	9264
JRI26	7355	8703	6321	7486
JRI29	7107	7067	6159	6083
JRI35	7000	8081	6019	6955
JRI49	20909	18739	17951	16096
JRI50	16309	18851	14004	16192
JRI62	8351	10670	7178	9178

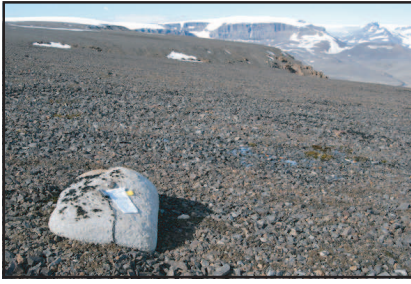
Table 3

*Figure





***Figure**



Sample: JRI 49 Lithology: Granite
Altitude: 360 m Age: 17.7 ± 0.8
Context: Lachman Mesa on hyaloclastite blockfield.



Sample: JRI 50 Lithology: Granite
Altitude: 370 m Age: 15.1 ± 0.4
Context: Lachman Mesa on hyaloclastite blockfield.



Sample: JRI 33 Lithology: Basalt
Altitude: 312 m Age: 19.9 ± 7.3
Context: Near Davies Dome. Basalt-rich drift.



Sample: JRI 34 Lithology: Basalt
Altitude: 244 m Age: 22.1 ± 6.6
Context: Near Davies Dome. Basalt-rich drift.



Sample: JRI 26 Lithology: Granite
Altitude: 170 m Age: 6.7 ± 0.3
Context: San Jose pass. Interior ice sheet.



Sample: JRI 29 Lithology: Granite
Altitude: 25 m Age: 6.1 ± 0.3
Context: St. Martha Cove. LGM moraine fragment. Interior ice sheet.



Sample: JRI 01 Lithology: Granite
Altitude: 104 m Age: 12.2 ± 0.4
Context: San Carlos Hill. Coastal erratic-rich drift.



Sample: JRI 03 Lithology: Granite
Altitude: 103 m Age: 11.3 ± 0.4
Context: San Carlos Hill. Coastal erratic-rich drift.



Sample: JRI 09 Lithology: Granite
Altitude: 39 m Age: 8.9 ± 0.2
Context: Sharp Valley. Coastal erratic-rich drift.

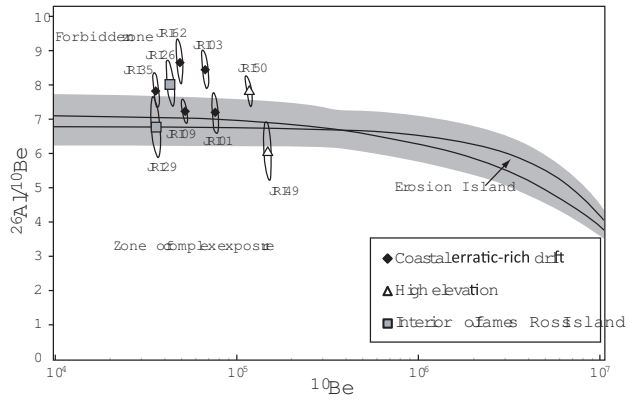


Sample: JRI 35 Lithology: Granite
Altitude: 45 m Age: 6.3 ± 0.2
Context: Cape Lachman. Coastal erratic-rich drift.



Sample: JRI 62 Lithology: Granite
Altitude: 144 m Age: 7.6 ± 0.3
Context: LGM moraine fragment on erratic-rich drift, Kaa Bluff. Coastal erratic-rich drift.

*Figure



*Figure

